Research Article | Vol. 31, No. 23 / 6 Nov 2023 / Optics Express 37437
Optics EXPRESS

Out-of-plane multilayer-dielectric-grating compressor for ultrafast Ti:sapphire pulses

CHRISTIAN M. WERLE,[1,*] CORA BRAUN,[1,2] TIMO EICHNER,[1,2] THOMAS HÜLSENBUSCH,[1,2] GUIDO PALMER,[1] AND ANDREAS R. MAIER[1]

[1]*Deutsches Elektronen-Synchrotron DESY, Notkestr. 85, 22607 Hamburg, Germany*
[2]*Department of Physics, Universität Hamburg, Luruper Chaussee 149, 22761 Hamburg, Germany*
[*]*christian.werle@desy.de*

Abstract: Extreme heat loads on optics, in particular the final pulse compression gratings, are a major hurdle to overcome in the ongoing push towards high average power (kW) and high repetition rate (kHz) operation of terawatt-class Ti:sapphire lasers. Multilayer dielectric (MLD) diffraction gratings have been suggested as a potential alternative to traditionally gold-coated compressor gratings, which are plagued by high energy absorption in the top gold layer. However, to support the required bandwidth (and ultimately the desired pulse duration) with MLD gratings, the gratings have to be operated in an out-of-plane geometry near the Littrow angle. Here, we report on the design of an MLD-based out-of-plane test compressor and a matching custom stretcher. We present a full characterization of the MLD compressor, focusing on its spectral transmission and the significance of laser pulse polarization in the out-of-plane geometry. To demonstrate compression of 40 μJ pulses centered at 800 nm wavelength to 26 fs pulse duration, we use the compressor with an MLD and gold grating configuration, and fully characterize the compressed pulses. Extrapolating our results indicates that MLD-grating-based out-of-plane compressors can support near-transform-limited pulses with sub-30 fs duration and good quality, demonstrating the viability of this concept for kW-level ultrafast Ti:sapphire laser systems.

1. Introduction

High-power lasers based on the Ti:Sapphire (Ti:Sa) architecture are versatile tools providing ultrafast laser pulses with peak powers up to 10 PW [1–3]. They enable a plethora of applications, including laser-driven particle acceleration (LPA) [4,5] and high-field QED [6,7]. While these systems can reach impressive peak powers, their pulse repetition rate has so far been limited to typically a few Hz. Significantly higher repetition rates are desirable not only to enable high throughput applications and better statistics in experiments, but also to deploy fast active stabilization [8] and experiment-to-driver feedback. On the path towards high repetition rate (kHz) and high average power (kW) Ti:Sa lasers, progress on three crucial technologies is required: (i) pump lasers with kHz repetition rate as well as (ii) amplifier architectures and (iii) pulse compressor gratings that scale well to kW-average power. The community is actively addressing those challenges.

While most TW- and PW-class laser systems today are still pumped by flashlamp-based lasers, which are effectively limited to a few-Hz repetition rate, diode-based pump lasers that offer better thermal management, higher energy efficiency, and higher repetition rates are becoming available. First systems based on diode pump lasers have been commissioned [2] or are being planned [9]. Novel pump lasers are being developed [10,11].

#501093 https://doi.org/10.1364/OE.501093
Journal © 2023 Received 20 Jul 2023; revised 9 Oct 2023; accepted 10 Oct 2023; published 23 Oct 2023

Optics EXPRESS

The relatively high quantum defect of Ti:Sa is associated with complex thermal management and effects like thermal lensing, deformation and stress that all scale with average power. With most high-intensity Ti:Sa systems today operating at an average power of a few-10 W, efficient cooling schemes and new amplifier architectures will be crucial for future kW-level amplifiers. Concepts currently under consideration include thin-disk Ti:Sa amplifiers [12,13], thin-slab Ti:Sa amplifiers [14,15], as well as gas-cooled multislab amplifiers [16,17] that have been developed for different gain media.

The final compressor gratings in Ti:Sa lasers typically feature a gold coating to support sufficient bandwidth for ultrashort pulses. However, around 3%-5% of the incident laser power [18] is absorbed by the gold layer, which can lead to heat-induced deformation of the grating substrate and spatio-temporal couplings deteriorating the pulse quality. These effects can become relevant already at a few-10 W of average power [19,20]. To overcome this limitation, several concepts to actively cool the compressor gratings have been proposed [21,22].

A more fundamental path to reduce the heat load on the compressor gratings would be the use of multilayer dielectric (MLD) diffraction gratings, as MLD coatings have a drastically lower absorption compared to gold. However, such gratings were previously limited in bandwidth to 30-40 nm due to guided mode resonances and were thus mainly used in Nd:glass lasers aiming for pulse lengths of several 100s of fs. Only recently, coatings were designed and test gratings were manufactured that support the broad spectra of ultrafast Ti:Sa lasers [23,24]. To maximize the bandwidth, these gratings have to be operated close to Littrow angle and thus in a rather unconventional out-of-plane configuration [23–25].

A first compressor based on these initial test gratings was described by Alessi *et al.* [26,27] and Link *et al.* [28]. References [26–28] confirmed that the out-of-plane design has no inherent detrimental effects on the temporal pulse structure and that the spectral dispersion is similar to a gold-grating based compressor. Furthermore, they experimentally verified a spectral transmission of around 90%, highlighting the potential to support high-average-power laser operation. The test compressor [26–28], however, was operated with a mismatched stretcher and the gratings did not have the necessary size to fully support the dispersed laser spectrum (on the second and third grating). Therefore, the resulting pulses were not fully compressed and the ultimate compression performance could only be estimated. Thus, to the best of our knowledge, no demonstration of near-Fourier-limited pulses from a compressor using MLD gratings for Ti:Sa lasers has been presented so far.

Here, we report on the design and experimental verification of an MLD-based test compressor in an out-of-plane configuration supporting ultra-fast Ti:Sapphire laser pulses. We discuss a matching stretcher design, which is based on transmission gratings, and experimentally demonstrate stretching and recompression of sub-30-fs pulses with a combination of MLD and gold gratings. Finally, we characterize the spectral efficiency of the MLD compressor, as well as the temporal contrast and the polarization of the compressed pulses. Our results indicate that MLD-grating-based compressors in an OOP configuration can support high-quality near-Fourier-limited pulses pulses, showing the viability of this concept to support future kW-level ultrafast Ti:Sa lasers.

2. Stretcher and compressor concept

The high diffraction efficiency and low absorption typically associated with MLD gratings render them an attractive option for high average power ultrafast laser pulse compressors. Due to the multilayer-based reflection and diffration process, however, these gratings only provide high efficiencies over a large spectral bandwidth, if they are used with angles of incidence (AOI) close to Littrow incidence [23], which is around 36° for 800 nm Ti:Sa beams and typical line densities of 1480 lines/mm. This results in very small angles between the incoming and outgoing beam, especially for the central wavelengths. For geometrical reasons, the typical compressor

Optics EXPRESS

layout, where all beams propagate in only one plane, cannot be used. Instead, an out-of-plane geometry is required to have a clip-free propagation through the compressor [24,25,29]. Here, the gratings are rotated by a small angle either around their pitch or roll axis (or both). This sends the diffracted beam out of the diffraction plane, leading to the required separation between input and output beam. The amount of out-of-plane tilt is effectively limited by the required compressor bandwidth, as larger angles lead to an increasingly narrow diffraction efficiency. For typical bandwidths required for the compression of ultrafast Ti:Sa laser pulses, out-of-plane angles are on the order of a few degrees, leading to small (but still workable) beam deviation angles of around 10°. Due to this overall very limited design space, the MLD coating design and the angles of incidence derived from it largely define the layout of an MLD-grating-based compressor.

2.1. Compressor layout

Figure 1 shows the basic configuration of a four-grating out-of-plane compressor. The out-of-plane angle δ, realized here by a pitch angle of $\delta/2$, introduces the vertical beam displacement necessary for the beams to pass over the first and last of the compressor gratings. With the out-of-plane angle limited by the desired bandwidth, the compressor requires a minimum amount of grating separation to achieve a certain height step. The size of the gratings and thus the required beam separation depend on the beam size, which for high-power laser systems is basically governed by the desired pulse energy in combination with the damage threshold of the gratings. In this sense, the final pulse energy of the laser defines a minimum amount of dispersion that the compressor will generate or, in other words, a minimum pulse duration (stretching factor) of the laser pulse before the compressor.

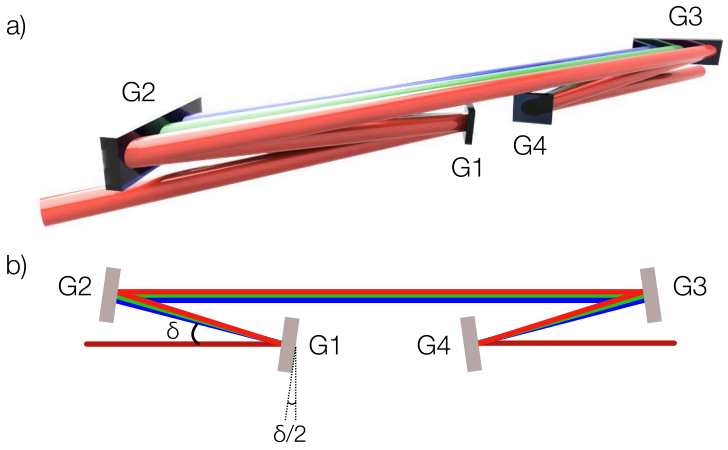

Fig. 1. 3D-render (a) and side-view (b) of a four-grating out-of-plane compressor. The gratings are oriented in Littrow angle to the incoming beam. An additional small pitch angle $\delta/2$ sends the diffracted and dispersed beam out of the plane of the incoming beam and creates the height step for the beam to pass G1 and G4. The blue, green and red beams illustrate the spectral separation within the compressor.

Exemplary, we check the feasibility of the out-of-plane pulse compressor concept for a 100 TW class Ti:Sapphire laser, delivering 3 J in 30 fs pulse length [30]. Operated at high repetition rate, such a system would be an ideal driver for laser-plasma acceleration. Using the raytracing-software ZEMAX, we model a potential OOP compressor for these laser parameters. For the MLD gratings, we assume a laser damage threshold similar to gold-coated gratings [24], i.e., around 100 mJ/cm^2. Operating the compressor with a fluence of 30 mJ/cm^2, 1480 lines/mm

Optics EXPRESS

gratings, and 3.8° out-of-plane angle, we would require a separation of 1770 mm between the two grating pairs to achieve the necessary height step.

We use ZEMAX to model the beam diffraction for this compressor setup within the spectral range of 750 – 850 nm and thus calculate its spectral phase, shown in Fig. 2(c). It generally follows the typical near-parabolic shape of a compressor that applies predominately GDD. It actually yields the exact same spectral phase as an in-plane Treacy compressor with the same AOI but a slightly higher grating line density. As such, an OOP compressor can be used completely analogous to a conventional in-plane version, without any conceptual complication to the temporal layout of the CPA laser system. In this example configuration, the compressor yields a dispersion of -1.07×10^7 fs^2, and a corresponding stretched pulse duration of 1.1 ns for a 35 nm bandwidth beam, which is in line with typical stretching factors in large-scale Ti:Sa lasers.

2.2. Stretcher layout

For optimum compression, the spectral phase of the incoming beam must match the phase applied by the compressor. We consider the compressor design as fixed due to the constraints imposed by the MLD design, and therefore adapt the stretcher to the requirements set forth by the compressor. As mentioned above, the OOP compressor phase is equivalent to that of an in-plane compressor with slightly altered grating line density. The matching process is thus equivalent to a normal in-plane case, with generally the same operations and scaling.

To facilitate this matching process, we combine the phase data of the compressor derived from its ZEMAX model with analytical descriptions [31] for the spectral phase shift of an Oeffner-type stretcher [32] to create a custom matching script that can calculate the grating parameters and dimensions of an optimally matched stretcher.

Please note, that in the following we will neglect additional dispersion, that would be present in the optical path of a real laser system between stretcher and compressor. This assumption seems to be well justified, as the dispersion caused by the stretcher is typically much larger than the combined dispersion caused by all transmissive optics, e.g., lenses, crystals, and so on. Accounting for this additional dispersion would only slightly alter the stretcher design.

Based on our calculations, we find that the optimum stretcher has – not surprisingly – almost the same grating period and AOI as the corresponding compressor and the stretcher gratings would also have to be operated at Littrow angle. Deviating from this optimal case, for example by using significantly different line densities and input angles to avoid the Littrow incidence, would seriously degrade the phase matching over the large spectral bandwidth required for ultrashort laser pulses. While a rough matching to minimize at least the overall GDD of the CPA system close to the center wavelength would still be possible, it would result in a significant mismatch in the higher phase orders, leading to sub-optimal compression. A stretcher based on reflective gratings would therefore necessitate an out-of-plane geometry as well.

This geometry can, however, be avoided by using transmission gratings, which naturally separate the incoming and outgoing beams on opposite grating sides. With transmission gratings, we can use a standard in-plane Oeffner telescope geometry for the stretcher, which minimizes aberration while using conventional spherical optics [32]. We thus propose a 2-transmission-grating-based Oeffner stretcher in a double-pass configuration as shown in Fig. 2(a)) and b) to match the stretcher dispersion to the out-of-plane compressor configuration.

The double-pass setup allows the stretcher to generate enough dispersion to fit the large compressor, while limiting the gratings to a commercially available size. The 2-grating configuration in combination with the Oeffner-type telescope makes the setup almost fully aberration-free (if perfectly aligned). Especially with the double-pass configuration, minimization of aberrations becomes increasingly important, as these otherwise add up over the passes and compromise the pulse and beam quality.

Optics EXPRESS

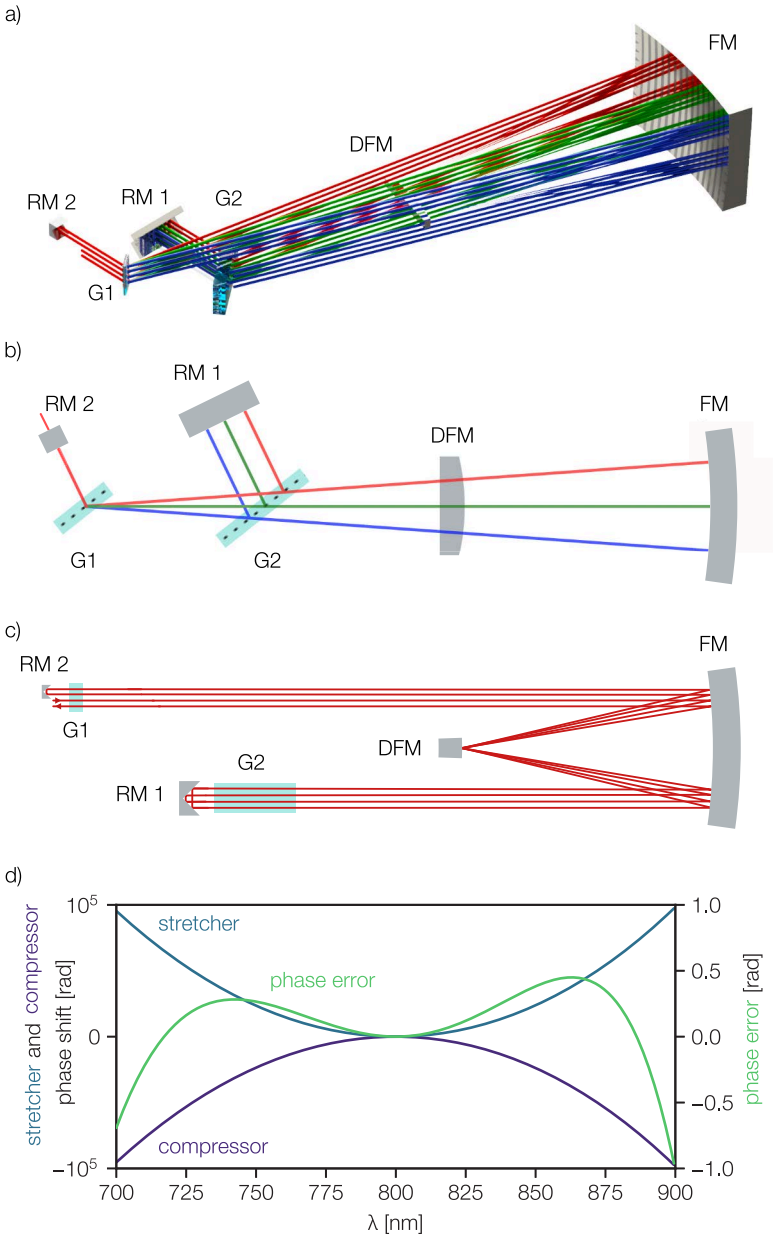

Fig. 2. 3D-render (a), top-view (b), and side-view (c) of the 2-transmission-grating stretcher setup. The first grating G1 is positioned at the center of curvature of both the focusing mirror (FM) and defocusing mirror (DFM). This ensures that beams of equal wavelength are stacked perfectly on top of each other in the stretcher passes. The separation of the second grating (G2) from G1 creates the necessary dispersion for the pulse stretching. The figures show the large roof mirror (RM1) that sends the spatially chirped beam back into the setup and the small roof mirror (RM2) used to force a double-pass of each pulse through the stretcher. (d) Spectral phase calculated for a matched stretcher (blue) and compressor (violet) pair, derived from raytracing trackings of the compressor and the analytical model of the stretcher. Proper matching results in a 4th-order polynomial residual phase error (green) of <1 rad.

Optics EXPRESS

Figure 2(c) shows the spectral phase of a matched stretcher and compressor pair using the analytical model discussed above. Here, only the stretcher grating separation and AOI were considered free parameters, which results in a minimization of the second-order (GDD) and third-order dispersion (TOD) after the compressor. The residual phase mismatch is therefore a fourth-order polynomial, which shows <1 rad phase error over the whole required spectral range (750 nm to 850 nm). Further improvement of the matching is possible by allowing the matching algorithm to freely choose the stretcher grating period to minimize the fourth order of the residual phase. For our conceptual study, we opted to keep the readily available grating period of 1480 lines/mm.

A similar stretcher design using a 2-transmission-grating stretcher in combination with a gold-grating-based OOP compressor was previously proposed and implemented at the Rutherfold-Appleton-Laboratory by Tang *et al.* [33]. The setup differs from ours as it does not use a Oeffner telescope in the stretcher, but only a single focusing mirror. The main goal of [33] was to limit phase noise and the degradation of the temporal contrast assicoated with it. Therefore, the reflection in the Fourier plane of the stretcher, i.e., on the small defocusing mirror of the Oeffner telescope, which can lead to spectral phase noise [34], was avoided.

However, a full Oeffner telescope design has the benefits of reduced aberrations in the beam and also allows for a fully in-plane geometry on the gratings, making tuning easier. Furthermore, it has been shown experimentally that higher surface quality mirrors in the stretcher can significantly reduce temporal contrast degradation [35,36]. For these reasons, we decided to still go for a transmission grating stretcher with Oeffner telescope.

3. Stretcher and compressor demonstrator setup

Based on these basic stretcher and compressor design considerations, we built a demonstrator setup to test its performance and to evaluate technical challenges that could arise from the MLD gratings operated in the OOP geometry. The conceptual layout of our test setup is shown in Fig. 3. We used pulses of $\approx 40\ \mu J$ centered at 800 nm with a typical bandwidth of 60 nm FWHM from a recently commissioned white-light seeded OPCPA laser [37] built by our group and designed to seed a Ti:Sa CPA system. The pulses were not fully compressed at the laser output, but slightly chirped to about 220 fs FWHM pulse duration. The beam diameter was about 1 mm FWHM.

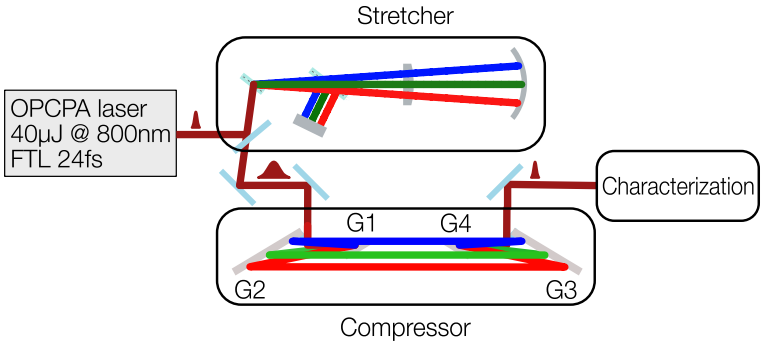

Fig. 3. Overview of the experimental setup used for the pulse recompression tests. The OPCPA provides slightly chirped seed pulses centered around 800 nm that are fed into the custom stretcher and compressor. The recompressed pulses are carefully analyzed with a scanning long-pulse autocorrelator (PulseCheck), a Grenouille, a Wizzler, and a third-order auto-correlator (Tundra) to measure the pulse length, shape, and contrast.

The pulses were then stretched by an Oeffner stretcher using two transmission gratings. The Oeffner telescope had a primary radius of curvature of 1.0 m. To achieve the necessary

Optics EXPRESS

stretcher-to-compressor matching, the 1480 lines/mm transmission gratings were used at an AOI of 36.3°. To emulate the beam aberrations and alignment challenges of a full-size system, the setup was built in the double-pass configuration, with the laser pulses hitting each of the two gratings four times. The setup stretched the pulses to roughly 270 ps. This stretching factor was mainly chosen to keep the footprint of the subsequent compressor reasonably compact and to reduce the compressor grating size. For a full-size amplifier system, the applied dispersion would likely increase by a factor of 2 to 4.

The OOP test compressor was built with a set of 1480 lines/mm custom MLD gratings. They were designed to efficiently diffract 800 nm pulses at an AOI of 36.3°. To achieve the necessary OOP angle, the gratings were first rotated by $\delta/2 = 3.82°$ (see: Fig. 1) around their pitch axis (the axis in the grating surface and perpendicular to the grating lines). Then, the 36.3° rotation around the grating yaw axis, meaning the axis of the grating lines, was applied to reach the Littrow incidence. This specific OOP alignment procedure is described as "Lab" configuration in [25]. The grating distance was scanned to reach optimum compression.

We operated the compressor in two different configurations. We studied the effect of the out-of-plane geometry on the laser polarization with a set of four MLD gratings (G1-G4). In the following, we refer to this setup as the pure-MLD compressor.

The four MLD gratings, that were available during the measurements, were, however, limited in size. In particular, their width was too small to support the full bandwidth (60 nm) of the dispersed beam on G2 and G3. In a second configuration, we therefore installed two gold-coated gratings of sufficient size (Spectrogon; 1480 lines/mm; 50mm x 140mm; NIR Au-coating), replacing grating G2 and G3. We refer to this configuration as hybrid compressor. We used the hybrid compressor for the characterization of the temporal pulse properties.

Since the spectral efficiency of the gold gratings is very broadband, the overall transmission of the compressor in the hybrid configuration is still dominated by the performance of the MLD gratings. To properly capture the effect of the gold gratings and extend the spectral efficiency characterization of the pure-MLD setup towards longer and shorter wavelengths, the spectral transmission was measured in both configurations (pure-MLD and hybrid) and the measurements were combined. As we will show below, the gold gratings have only a minor effect on the compressed pulse duration, and do not compromise the general findings of our work.

4. Experimental characterization of the system

To demonstrate the performance of the transmission grating stretcher in combination with an MLD-grating compressor, we characterized the output pulses with a variety of diagnostics: We measured the spectral transmission of both compressor configurations (pure and hybrid), as well as the pulse duration, the contrast, and the polarization state of the compressor output pulses. The results of these measurements are presented in the following.

4.1. Spectral efficiency

With the supported bandwidth being one of the major obstacles in the development of the MLD gratings, the width of the spectral transmission of both the stretcher and compressor are essential for the viability of our setup. Furthermore, multilayer gratings should, in principle, offer an overall higher diffraction efficiency compared to gold gratings [24], which would reduce losses in the compressor and thus save expensive pump power. The experimentally verified compressor transmission is thus an important figure of merit.

Figure 4(a) and 4(b) show the measured spectral efficiencies of the stretcher and compressor setup, respectively. All spectra were measured using a fiber-coupled spectrometer with an integrating sphere. To determine the spectral efficiency over a range from 750 to 850 nm, we tuned our OPCPA to three different central wavelengths and then combined the measurements. We characterized the spectrum before the stretcher, before the compressor, and after the compressor.

Optics EXPRESS

For comparison with our experimental data, we show the theoretically expected efficiencies (dashed green lines) based on calculated grating performance (supplier data).

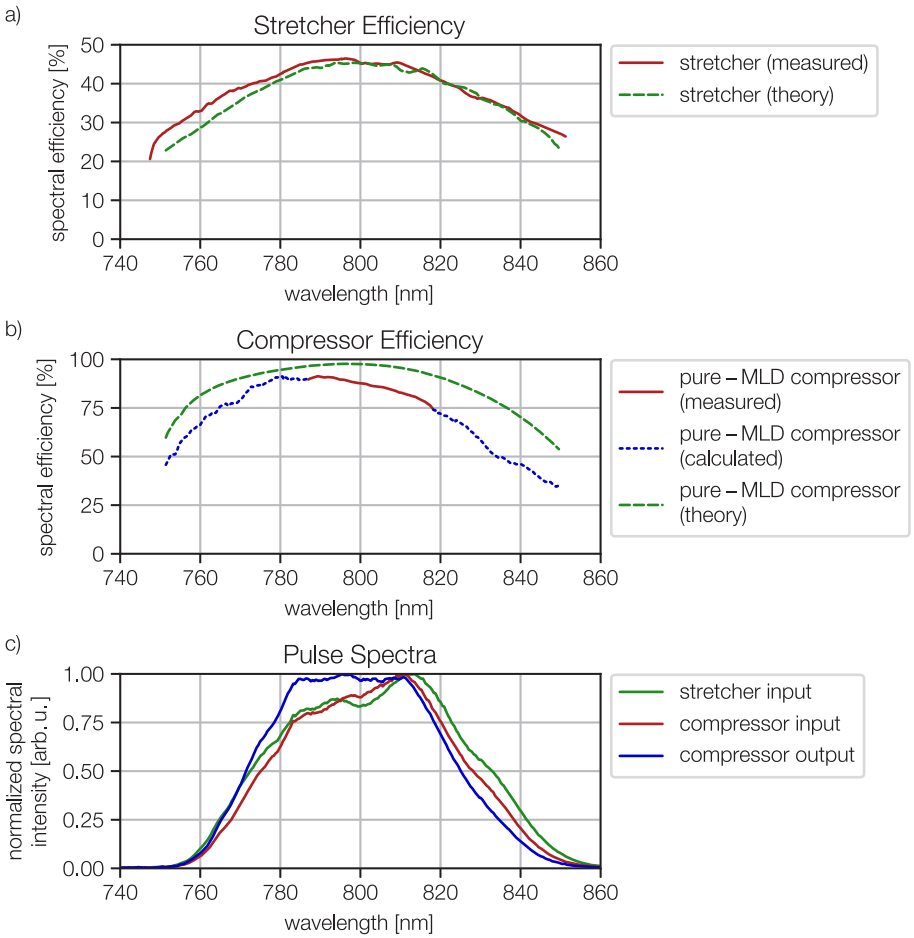

Fig. 4. Spectral efficiency (measured and calculated) of stretcher (a) and compressor (b). The MLD compressor efficiency was measured in the pure-MLD configuration in the central wavelength region (red solid line) and calculated using the hybrid configuration measurement results, corrected for the well-known spectral efficiency of the gold gratings (blue dotted line). Each curve is averaged over 200 individual measurements. (c) Exemplary pulse spectra (normalized) before the stretcher, before the compressor, and after the compressor.

The stretcher spectral efficiency, Fig. 4(a), fits well to the theoretical prediction. At 46.5%, the peak efficiency is comparably low – it is a result of the double-pass configuration, that includes eight grating passes. A larger stretcher setup using bigger transmission gratings that could generate enough dispersion in a single pass could increase the overall efficiency by reducing the number of grating passes. However, as the pulse energy in the stretcher is still low, losses here are typically more acceptable, as they are easier to recover than later in the amplifier chain.

The spectral efficiency of the MLD compressor is shown in Fig. 4(b). In a ~ 35 nm bandwidth, the efficiency was characterized using the pure-MLD compressor (solid red line), i.e., with four MLD gratings. Due to the limited size of these first sample gratings, the spectrum outside this range was clipped on grating G2 and G3 inside the test compressor. To extend the characterization of the MLD compressor to the full bandwidth from 750 nm to 850 nm, we repeated the spectral

Optics EXPRESS

efficiency measurement with the hybrid compressor. We then corrected these results for the (well-known) spectral efficiency of the gold gratings to derive the expected performance of the pure-MLD compressor (blue dotted line).

From these combined measurements, we can see that the general shape of the spectral efficiency curve of the MLD compressor is similar to the predicted design efficiency (dashed green line) and reaches a FWHM bandwidth of 89.1 nm. In contrast, the absolute compressor efficiency is lower than predicted from the grating design. Especially towards longer wavelengths, the compressor deviates from the expected performance. This could possibly be caused by manufacturing imperfections that typically lead to a spectral efficiency $\eta(\lambda)$ about 1%-2% lower than the design. This results in significant deviations (η^4) after four gratings. With improvements in grating design and manufacturing, however, it should be possible to recover some of the lost performance in future designs.

Nevertheless, the measured peak spectral transmission of the compressor is 91.3% even with the present grating imperfections, compared to the 70-75% typically expected for a gold grating compressor. The integrated spectral transmission, i.e., the pulse energy transmission, is 80%, for a laser pulse with the compressor input spectrum shown in Fig. 4(c) (red line). These results confirm the potential of MLD-grating-based compressors for high energy ultrafast Ti:sapphire lasers.

Figure 4(c) shows the laser pulse spectrum measured at the stretcher input, compressor input, and compressor output. These measurements were performed with the hybrid compressor. The stretcher slightly reduces the bandwidth by 7.5 nm, while still preserving the overall spectral shape. In contrast, the compressor slightly alters the output spectrum to a more flat-top shape, while still preserving the FWHM pulse bandwidth of 53 nm. In a full MLD compressor, we would expect a slight narrowing to 50 nm for the same input spectrum due to the slightly narrower compressor transmission. The effect of this narrowing on the pulse duration will be discussed in the following section.

4.2. Pulse duration and shape

To fully compress the laser pulse after the stretcher and compressor, both setups had to be tuned such that the overall GDD and TOD were minimized. This required adjusting the AOI and grating separation of stretcher and/or compressor so they would be properly matched. We chose to tune the stretcher grating AOI rather than the compressor angle, as the compressor MLD grating design limits the possible incidence angles under which efficient diffraction is possible to sub-1°. In contrast, the acceptance angle for the transmission gratings in the stretcher was about 3°. Furthermore, the stretcher has only two gratings to tune instead of four and in-plane symmetry that retains the alignment under angle tuning, making the tuning easier in practice. After each stretcher angle adjustment, we tuned the compressor grating separation for the minimal reachable pulse duration, until an overall optimum was reached.

With this matching strategy, we were able to successfully recompress the pulses from our OPCPA seed laser to a near-Fourier-limited sub-30 fs FHWM duration without any additional active dispersion tuning, like using an acousto-optic programmable dispersive filter (e.g., Dazzler). In particular, we reached 25.9 ± 0.7 fs output pulses (compared to the average Fourier-limit of 25.1 ± 0.3 fs), shown in Fig. 5.

This measurement was taken with a Wizzler and recorded with 10 Hz data acquisition over 10 min. We confirmed these results with a Grenouille measurement. These results show that an MLD-grating-based compressor is fully capable of supporting ultrafast, well-compressed pulses.

The average phase was relatively flat, with the phase error being dominated by higher-order polynomials. The average TOD of $(1.0 \pm 0.2) \times 10^4$ fs^3 can likely be improved further with even more fine adjustment of the stretcher AOI or by using an acousto-optic programmable dispersive filter. Nevertheless, the overall flat phase shows, that the stretcher-to-compressor matching was

Optics EXPRESS

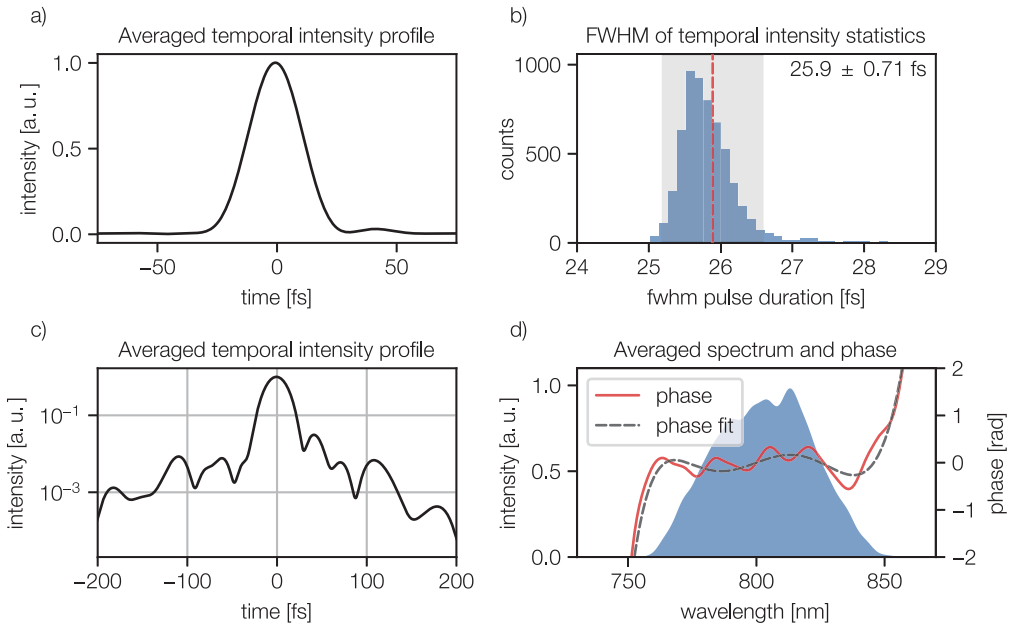

Fig. 5. Temporal pulse characterization: A data set of 6000 compressor output pulses was recorded with the Wizzler over ten minutes. The plots show the average pulse shape (a), the statistic distribution of the measured FWHM pulse duration (b), the residual side-peak structure in the fs contrast (c), as well as the average spectral intensity and phase (d). The average pulse phase fit resulted in a GDD of $(-7 \pm 72)\,\mathrm{fs}^2$, a TOD of $(1.0 \pm 0.2) \times 10^4\,\mathrm{fs}^3$, and an FOD of $(-1.4 \pm 0.5) \times 10^4\,\mathrm{fs}^4$. Measurements were taken with the hybrid compressor configuration.

successful, allowing for the short pulses. However, the short timescale contrast still reveals some higher-order errors, as can be seen in the logarithmic pulse shape plot. As the FOD and higher-order phase polynomials were relatively constant throughout the measurements, this likely hints at systematic imperfections in the coating dispersion of our optics or surface quality issues with the large reflective optics in the stretcher and compressor.

While this data was taken with the hybrid compressor, the further transmission bandwidth reduction of a full MLD system should only slightly lengthen the resulting pulse duration. To estimate this effect, we applied the estimated full-MLD transmission (Fig. 4(b)) to the spectrum measured at the compressor input. The Fourier-limit of this spectrum and thus the theoretically achievable pulse duration increases from 25.1 fs for the hybrid compressor to 25.8 fs for the full-MLD setup. So for a properly optimized stretcher and full-MLD compressor, we expect that the resulting pulse lengths should only increase by less than 1 fs. This suffices to provide ultrashort pulses for experiments.

4.3. Contrast

Additionally, we measured the ps-scale pulse contrast with a scanning third order autocorrelator, compare Fig. 6. No significant prepulses were present down to the noise level of 4.1×10^{-9}. The pulse did however show a notable post-pulse plateau and a ps-pedestal. As mentioned before, the latter is most likely linked to the surface roughness of the stretcher mirrors causing high-frequency phase noise. For the test experiments presented here, we used standard grade optics for ease of procurement, but with higher quality optics this should be improvable. Nevertheless, the intensity contrast values are comparable to other large-scale Ti:Sa systems. So while the compression

Optics EXPRESS

test setup was not specifically built nor optimized for the highest possible contrast, the current pulse contrast should already be sufficient for many applications, e.g., laser-plasma acceleration experiments.

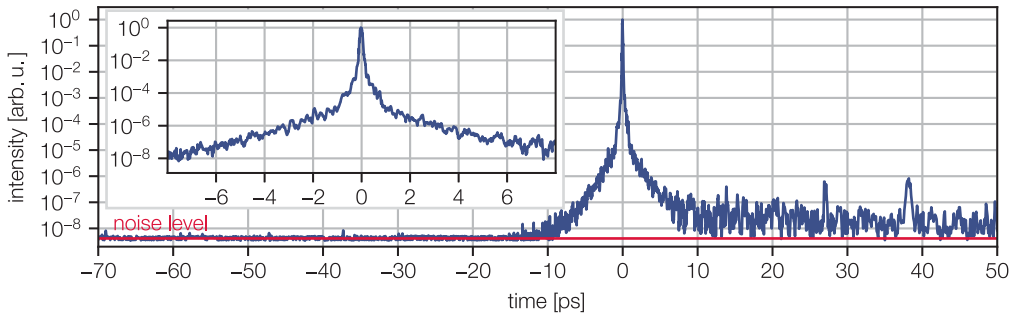

Fig. 6. Temporal contrast of the optimized recompressed pulse at the MLD compressor output, measured with a third-order scanning autocorrelator. The inset plot shows a zoomed in version of the trace to give a better view of the short term (few-ps) contrast, which is dominated by the main peak pedestal. The red line marks the average noise level of the measurement device. Measurements were taken with the hybrid compressor configuration.

4.4. Polarization purity

The influence of the out-of-plane configuration on the polarization purity is often a matter of concern: As the gratings are neither in an ideal s- or p-polarization configuration, the effect on the polarization state is not trivial and strongly depends on the exact EM-field orientation on the grating surface, specifically the orientation relative to the grating grooves. This orientation depends on the specific way the grating is rotated to achieve the required out-of-plane geometry. Different out-of-plane angle definitions were described in [25,29], with the three common angle configurations being referred to as "Roll", "Pitch" and "Lab". All three configurations are equivalent in terms of the relative positioning of the compressor gratings with respect to each other. However, they lead to a different orientation of the overall compressor in the lab frame. Switching between the configurations effectively corresponds to a rotation of the compressor around the beam input axis. Therefore, these three configurations mainly differ in how the laser beam polarization is oriented relative to the grating grooves.

As mentioned above, the test compressor setup was built based on the "Lab" angle definition. This means that the gratings (starting from normal incidence with vertical grating lines) were first pitched up or down, before the yaw angle was adjusted to reach the correct AOI. This combination of rotations ensures that for a vertically polarized input beam, the grating lines are as close to a pure s-polarization as possible.

To verify that the "Lab" configuration was the correct choice to reach the best compressor performance, as well as to investigate the general effect of the compressor geometry on the polarization state, polarimetry measurements of the compressor were conducted, using the pure-MLD compressor configuration. Figure 7(a) shows the test setup and Fig. 7(b) the measurement results.

The polarization of the incoming beam was tuned using a $\lambda/2$ waveplate and a first polarizer (P1) to various polarization angles relative to pure vertical polarization, which is equivalent to moving the compressor configuration away from the "Lab" configuration. Using a second polarizer (P2) behind the compressor, we analyzed the output polarization state. We measured the angle of the linear polarization compared to pure vertical polarization by searching for the P2 rotation angle of maximum transmission. We also measured the polarization contrast, i.e., the

Optics EXPRESS

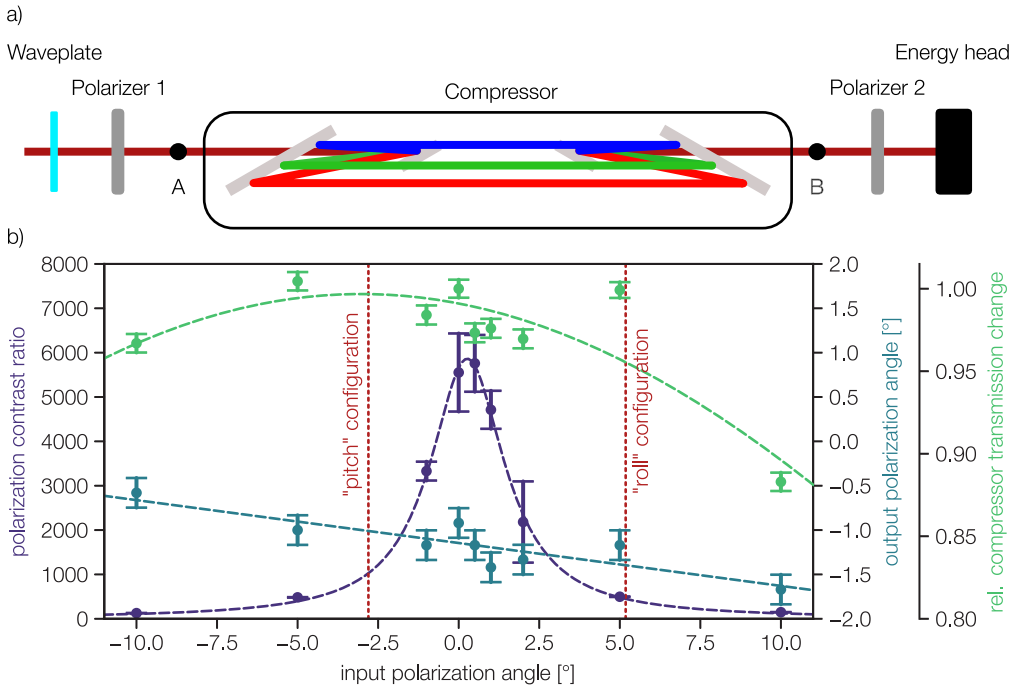

Fig. 7. (a) Setup for the polarimetry measurement: Polarizer 1 and the waveplate were used to tune the input polarization, while polarizer 2 was used to analyze the output polarization state behind the compressor by measuring the polarization contrast and net rotation angle. In addition, the energy head was placed in positions A and B to record the compressor transmission for different input polarizations. (b) Polarimetry measurement results, showing the polarization contrast (violet), the resulting output polarization angle (blue), and the relative change in the compressor transmission compared to 0° input. A Lorentzian, linear, and $\sin^4(2\alpha)$ are fitted to these data points, respectively. The dotted lines indicate the polarization angles equivalent to the "Pitch" and "Roll" configuration. Measurements were taken with the pure-MLD compressor configuration.

ratio between linear and circular polarization, by recording the maximum and minimum energy behind the output polarizer. In addition, we recorded the compressor transmission during the polarization scan.

Smith *et al.* discuss in [25] how the grating efficiency changes with the input polarization: the efficiency changes roughly with a sinusoidal behavior over a 180° rotation of the input polarization. We do observe only a slight change over the scanning range ±10°, with the efficiency dropping by up to 10% relative to the fully vertical polarization orientation (0°) and the changes in efficiency being a bit asymmetric. As the individual grating efficiency scales roughly sinusoidal, we fitted a $(a * \sin(2(\alpha - \alpha_0)) + c)^4$ to the measured data of the full compressor. Here a, c and α_0 are the fit constants for the efficiency modulation depth, average efficiency overall polarization and the polarization angle for the peak efficiency, respectively. The fit suggests the peak efficiency to be at $-3° \pm 1.4°$. According to [25], both the "Lab" and "Pitch" configuration should lead to a decent efficiency for a low-dispersion grating layout like our case of 1480 lines/mm gratings designed for 800 nm CWL. In contrast, the efficiency should start to dip for the "Roll" case. This is what we see in our measurements, where the efficiency optimum is roughly between the "Lab" and "Pitch" cases. Our fit suggests that the individual grating efficiency would decrease to about 50% close to p-polarization. While the limited angle scan range only allows for a rough estimate, this

Optics EXPRESS

result is good agreement with the model presented by Smith *et al.* [25]. Furthermore, the authors noted, that their efficiency simulations only included linear polarization states and neglected how elliptical polarization components would influence the efficiencies, remarking that this needed to be investigated in future work. As our experimental measurements naturally take these effects into account, the good agreement between their prediction and our measurements suggests that neglecting the elliptical polarization content should not have majorly affected their results.

Looking at the polarization contrast ratio, we find that it changes much more drastically with the input polarization, compared to the compressor transmission. Within our scan range, we found it to be dropping from 5760:1 to 127:1 when going away from a vertical input polarization. Using a Lorentzian fit, which seemed to best approximate the change in the polarization contrast, we find that the optimal contrast corresponds to an input polarization angle of $0.27° \pm 0.02°$ for our test setup. This small deviation from the pure "Lab" state might be the result of a potential minor misalignment of the compressor gratings in the test setup, shifting the optimum slightly. Nevertheless, the purity of the laser polarization state seems to be best conserved at or close to the "Lab" configuration. It is evident that the "Pitch" and "Roll" configurations would lead to significantly stronger elliptical/circular polarization contributions, increasing them in our case by a factor of 5 to 10. This clearly shows that the "Lab" configuration is the correct choice when a high polarization quality is required.

The orientation of the linear contribution of the output polarization stayed almost constant for all tested input polarization angles. It only changes by about $-0.05°$ per degree of input polarization rotation. Similar to normal in-plane gratings, the MLD gratings still act as polarizers, yielding a defined output direction. In our measurements, the polarization direction did deviate by about $-1°$, again likely due to the compressor not being set up perfectly.

In summary, we find that not only the grating efficiencies but also the purity of the laser polarization state are close to optimum when the compressor is set up in the "Lab" configuration, which makes it the best choice for optimal compressor performance. The polarization contrast is clearly the most affected laser property if the gratings are incorrectly oriented with respect to the laser polarization vector. The efficiency does vary with deviations between polarization and grating orientation, but is still close to optimum for "Lab". In principle, it would be possible to reach the same performance with other configurations by rotating the input polarization, effectively mimicking the "Lab" case. However, going away from a strictly vertical polarization would lead to further technical difficulties in the laser design, as this would lead to mixed states of s- and p-polarization in the adjacent parts such as folding mirrors. Therefore, "Lab" seems to be the clear choice based on our findings.

5. Discussion

In conclusion, we have built a setup combining an MLD grating based compressor in an out-of-plane configuration with a matched stretcher. We successfully stretched 800 nm, 40 µJ pulses from our OPCPA frontend to several hundred ps and then recompressed the pulses close to the Fourier-limit at below 26 fs with good ps-level pulse contrast. We investigated the effect of the OOP compressor geometry on the polarization state, showing that a polarization contrast exceeding 5000:1 is possible in the correct configuration. Integrated over the full pulse spectrum, the compressor transmission was about 80%, which demonstrates the potential of the MLD compressor to substitute conventional gold-grating-based compressors.

While we did not characterize the absorption by the coating of the specific MLD gratings installed in our setup, Alessi *et al.* [24] measured an absorption of 65 ppm for similar gratings. This absorption is several orders of magnitude lower than the absorption in conventional gold optics, and promises to effectively eliminate the issue of heat-induced substrate deformation for compressors operated at kW average power. Our results now confirm, that an actual pulse compressor with sufficient bandwidth to support sub-30-fs Ti:Sa pulses can be built using MLD

Optics EXPRESS

gratings. As we show, the out-of-plane configuration supports high-quality pulses. MLD grating based OOP compressors therefore are a viable alternative to traditional pulse compressors using gold-coated gratings, and open the path to future ultrafast Ti:Sappire lasers operated at kW average power.

Funding. Deutsche Forschungsgemeinschaft (491245950).

Acknowledgments. We acknowledge fruitful discussions with T. Erdogan at Plymouth Grating Laboratory, Inc. and J. Bromage at the Laboratory for Laser Energetics, University of Rochester. We appreciate support from the workshops and technical groups of DESY and the University of Hamburg.

Disclosures. The authors declare no conflicts of interest.

Data availability. Data underlying the results presented in this paper are not publicly available at this time but may be obtained from the authors upon reasonable request.

References

1. W. P. Leemans, R. Duarte, E. Esarey, S. Fournier, C. G. R. Geddes, D. Lockhart, C. B. Schroeder, C. Toth, J. Vay, and S. Zimmermann, "The BErkeley Lab Laser Accelerator (BELLA): A 10 GeV Laser Plasma Accelerator," AIP Conf. Proc. **1299**, 3–11 (2010).
2. E. Sistrunk, T. Spinka, and A. Bayramian, *et al.*, "All Diode-Pumped, High-repetition-rate Advanced Petawatt Laser System (HAPLS)," in *Conference on Lasers and Electro-Optics* (2017), paper STh1L.2.
3. F. Lureau, G. Matras, and O. Chalus, *et al.*, "High-energy hybrid femtosecond laser system demonstrating 2 × 10 PW capability," High Power Laser Sci. Eng. **8**, e43 (2020).
4. T. Tajima and J. M. Dawson, "Laser electron accelerator," Phys. Rev. Lett. **43**(4), 267–270 (1979).
5. E. Esarey, C. B. Schroeder, and W. P. Leemans, "Physics of laser-driven plasma-based electron accelerators," Rev. Mod. Phys. **81**(3), 1229–1285 (2009).
6. F. C. Salgado, K. Grafenstein, A. Golub, A. Döpp, A. Eckey, D. Hollatz, C. Müller, A. Seidel, D. Seipt, S. Karsch, and M. Zepf, "Towards pair production in the non-perturbative regime," New J. Phys. **23**(10), 105002 (2021).
7. L. Fedeli, A. Sainte-Marie, N. Zaim, M. Thévenet, J. L. Vay, A. Myers, F. Quéré, and H. Vincenti, "Probing strong-field qed with doppler-boosted petawatt-class lasers," Phys. Rev. Lett. **127**(11), 114801 (2021).
8. J. Natal, S. Barber, F. Isono, C. Berger, A. J. Gonsalves, M. Fuchs, and J. van Tilborg, "High-bandwidth image-based predictive laser stabilization via optimized Fourier filters," Appl. Opt. **62**(2), 440–446 (2023).
9. L. Gizzi, P. Koester, L. Labate, F. Mathieu, Z. Mazzotta, G. Toci, and M. Vannini, "A viable laser driver for a user plasma accelerator," Nucl. Instrum. Methods Phys. Res., Sect. A **909**, 58–66 (2018).
10. H. Chi, Y. Wang, A. Davenport, C. S. Menoni, and J. J. Rocca, "Demonstration of a kilowatt average power, 1j, green laser," Opt. Lett. **45**(24), 6803–6806 (2020).
11. C. Aleshire, T. Eichner, A. Steinkopff, A. Klenke, C. Jauregui, G. Palmer, S. Kuhn, J. Nold, N. Haarlammert, W. P. Leemans, T. Schreiber, A. R. Maier, and J. Limpert, "Frequency-doubled q-switched 4 × 4 multicore fiber laser system," Opt. Lett. **48**(8), 2198–2201 (2023).
12. V. Chvykov, H. Cao, R. Nagymihaly, M. P. Kalashnikov, N. Khodakovskiy, R. Glassock, L. Ehrentraut, M. Schnuerer, and K. Osvay, "High peak and average power ti:sapphire thin disk amplifier with extraction during pumping," Opt. Lett. **41**(13), 3017–3020 (2016).
13. R. S. Nagymihaly, H. Cao, D. Papp, G. Hajas, M. Kalashnikov, K. Osvay, and V. Chvykov, "Liquid-cooled ti:sapphire thin disk amplifiers for high average power 100-tw systems," Opt. Express **25**(6), 6664–6677 (2017).
14. V. Chvykov, "Ti:sa crystals in ultra-high peak and average power laser systems," Crystals **11**(7), 841 (2021).
15. V. Chvykov, H. Chi, Y. Wang, K. Dehne, M. Berrill, and J. J. Rocca, "Demonstration of a side-pumped cross-seeded thin-slab pre-amplifier for high-power ti:sa laser systems," Opt. Lett. **47**(14), 3463–3466 (2022).
16. A. Bayramian, P. Armstrong, and E. Ault, *et al.*, "The mercury project: A high average power, gas-cooled laser for inertial fusion energy development," Fusion Sci. Technol. **52**(3), 383–387 (2007).
17. P. D. Mason, M. Fitton, A. Lintern, S. Banerjee, K. Ertel, T. Davenne, J. Hill, S. P. Blake, P. J. Phillips, T. J. Butcher, J. M. Smith, M. De Vido, R. J. S. Greenhalgh, C. Hernandez-Gomez, and J. L. Collier, "Scalable design for a high energy cryogenic gas cooled diode pumped laser amplifier," Appl. Opt. **54**(13), 4227–4238 (2015).
18. O. Loebich, "The optical properties of gold," Gold Bull. **5**(1), 2–10 (1972).
19. V. Leroux, S. W. Jolly, M. Schnepp, T. Eichner, S. Jalas, M. Kirchen, P. Messner, C. Werle, P. Winkler, and A. R. Maier, "Wavefront degradation of a 200 tw laser from heat-induced deformation of in-vacuum compressor gratings," Opt. Express **26**(10), 13061–13071 (2018).
20. V. Leroux, T. Eichner, and A. Maier, "Description of spatio-temporal couplings from heat-induced compressor grating deformation," Opt. Express **28**(6), 8257–8265 (2020).
21. D. A. Alessi, P. A. Rosso, H. T. Nguyen, M. D. Aasen, J. A. Britten, and C. Haefner, "Active cooling of pulse compression diffraction gratings for high energy, high average power ultrafast lasers," Opt. Express **24**(26), 30015–30023 (2016).
22. E. P. Power, S. Bucht, K. R. P. Kafka, J. Bromage, and J. D. Zuegel, "Design and characterization of flow-cell integrated-flow active cooling for high-average-power ceramic optics," Opt. Express **30**(23), 42525–42540 (2022).

Optics EXPRESS

23. T. Erdogan, "Gratings for High-average-power Ti:Sapphire Laser Systems," Tech. rep., Plymouth Grating Laboratory (2018).
24. D. Alessi, H. Nguyen, J. Britten, P. Rosso, and C. Haefner, "Low-dispersion low-loss dielectric gratings for efficient ultrafast laser pulse compression at high average powers," Opt. Laser Technol. **117**, 239–243 (2019).
25. D. L. Smith, S. L. Erdogan, and T. Erdogan, "Advantages of out-of-plane pulse compression gratings," Appl. Opt. **62**(13), 3357–3369 (2023).
26. D. Alessi, "High-Average-Power Diffraction Pulse-Compression Gratings Enabling Next-Generation Ultrafast Laser Systems," LDRD Annual Report (2016), LLNL-TR-707794.
27. D. A. Alessi, E. Sistrunk, H. T. Nguyen, P. A. Rosso, T. Spinka, M. D. Aasen, S. Herriot, J. A. Britten, and C. Haefner, "A Compressor for High Average Power Ultrafast Laser Pulses with High Energies," in *Conference on Lasers and Electro-Optics* (Optica Publishing Group, 2017) paper STh1L.3.
28. E. F. Link, D. A. Alessi, L. C. Haefner, and J. A. Britten, "Symmetric out-of-plane configurations of diffractive gratings and method," US Patent US-10594106-B2 (2020).
29. G. Kalinchenko, S. Vyhlidka, D. Kramer, A. Lerer, and B. Rus, "Positioning of Littrow mounted gratings in pulse compressors," in *Optical Systems Design 2015: Optical Design and Engineering VI*, vol. 9626 (2015), p. 96261R.
30. KALDERA project at DESY, http://kaldera.desy.de. Accessed: 2023-06-08.
31. J. Jiang, Z. Zhang, and T. Hasama, "Evaluation of chirped-pulse-amplification systems with Offner triplet telescope stretchers," J. Opt. Soc. Am. B **19**(4), 678–683 (2002).
32. G. Cheriaux, P. Rousseau, F. Salin, J. P. Chambaret, B. Walker, and L. F. Dimauro, "Aberration-free stretcher design for ultrashort-pulse amplification," Opt. Lett. **21**(6), 414–416 (1996).
33. Y. Tang, C. Hooker, O. Chekhlov, S. Hawkes, J. Collier, and P. P. Rajeev, "Transmission grating stretcher for contrast enhancement of high power lasers," Opt. Express **22**(24), 29363–29374 (2014).
34. J. Bromage, C. Dorrer, and R. K. Jungquist, "Temporal contrast degradation at the focus of ultrafast pulses from high-frequency spectral phase modulation," J. Opt. Soc. Am. B **29**(5), 1125–1135 (2012).
35. L. Ranc, C. L. Blanc, N. Lebas, L. Martin, J.-P. Zou, F. Mathieu, C. Radier, S. Ricaud, F. Druon, and D. Papadopoulos, "Improvement in the temporal contrast in the tens of ps range of the multi-PW Apollon laser front-end," Opt. Lett. **45**(16), 4599–4602 (2020).
36. H. Kiriyama, Y. Miyasaka, and A. Kon, *et al.*, "Enhancement of pre-pulse and picosecond pedestal contrast of the petawatt J-KAREN-P laser," High Power Laser Sci. Eng. **9**, e62 (2021).
37. T. Eichner, T. Hülsenbusch, J. Dirkwinkel, T. Lang, L. Winkelmann, G. Palmer, and A. Maier, "Spatio-spectral couplings in saturated collinear opcpa," Opt. Express **30**(3), 3404–3415 (2022).